

Synthesis of Benzothiazole Derivatives Using Green Biobased Vitamin B₁ Supported on γ -Fe₂O₃@SiO₂ Nanoparticles as Catalyst and Insilico Antiviral Activity Screening

G Neelima^{1,3}, K Sesa Maheswaramma² and K Bhaskar Reddy^{3*}

¹Research Scholar, JNTUA, Ananthapuramu-515002, Andhra Pradesh, India

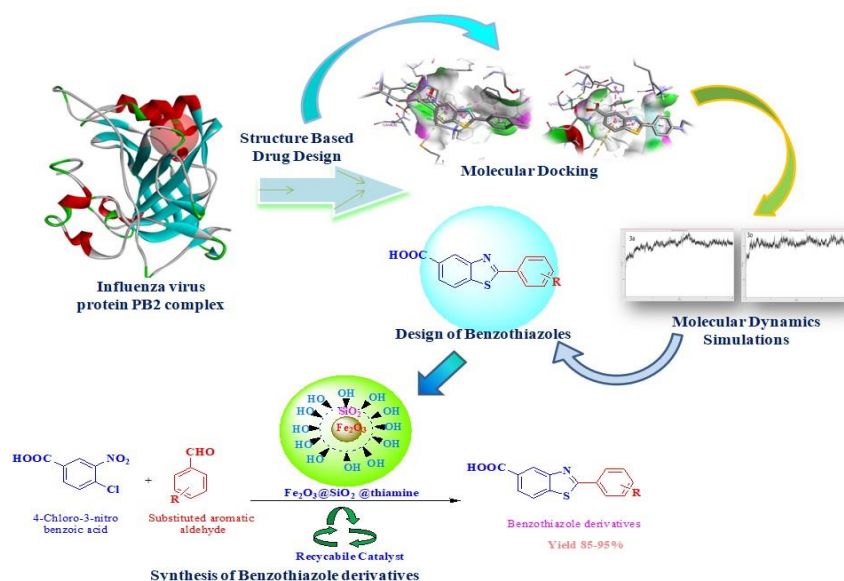
²Department of Chemistry, JNTUA College of Engineering (Autonomous), Pulivendula-516390, Andhra Pradesh, India

³Center for Pharmaceutical Nanotechnology, Sri Venkateswara College of Pharmacy (Autonomous), RVS Nagar, Chittoor-517127, Andhra Pradesh, India

Abstract

In the present research work, we report the synthesis of a series of benzothiazole derivatives synthesized and were docked for insilico studies against the influenza virus target. A novel biocompatible magnetic nanocatalyst was prepared by restraint of Vitamin B₁ (Thiamine hydrochloride) supported on the surface of silica- encapsulated γ -Fe₂O₃ nanoparticles. Vitamin B1 was covalently associated with the silica to indulge a nontoxic, inexpensive and biodegradable for the formation of complex with γ -Fe₂O₃. Magnetic bio-nanocatalyst were characterized by FT-IR, XRD, TEM analysis. However, this catalyst can be simply detached from the reaction mixture by using a magnetic field and directly recycled for five times without loss of its significant activity. The synthesized derivatives were structurally characterized with FT-IR, ¹H NMR and Mass spectra analysis. The antiviral activity and predicted insilico studies were prominent which revealed that compounds 3a and 3o illustrated better influenza virus inhibition as discriminated with the standard drug acyclovir. The efficacy of these synthesized benzothiazoles will need to be performing by in-vitro and in-vivo experiments as antiviral agents.

Graphical Abstract:



Key Words: Benzothiazoles, γ -Fe₂O₃@SiO₂ @ Vitamin B₁, Molecular modelling, Green catalyst, Magnetic properties.

1. Introduction

The development of competent, efficient and environmentally acceptable chemical procedures for the research of industrially relevant compounds and biologically active molecules is a major task for chemists in organic synthesis. A feasible and 'greener' bio based' method would accessible attention on use of ecofriendly non-toxic substances, use of ambient conditions, avoiding of destructive by-products and other wastes, as well as shortening of reaction times (Porfiri, 2020). To overcome the complications of inorganic compounds used such as mineral acid catalyst

such as (HCl and H₂SO₄) and solid acid catalyst like zeolites, clays, heteropolyacids and sulfated metal oxides. Due to inimical effects of corrosive lewis acids and protic acids on the environment, several alternative green methods have been investigated viz nanoparticles, ionic liquids and organocatalyst (Choghamarani, 2016). Therefore, the utilization of eco friendly organic molecules such as organo nanocatalyst has staggeringly increased in chemical research. In recent times, heterogenous coated magnetic nanoparticles have raised as a potent catalysts due to many advantages like readily availability, excellent stability, and biodegradable catalytic efficacy of immobilization of organo nanocatalyst because of their high surface to volume ratio (Zhang 2019).

Vitamin B₁ (VB₁) structure consists of pyrimidine and thiazole ring joined by Methylene Bridge (Figure 1) (Roger, 2009, Gurav, 2020 and Aghapoor, 2011). Moreover the usage of thiazoles as important catalytic efficacy for different organic transformations was studied (Azizi, 2014, Darabi, 2012, Choghamarani, 2016 and Rafiee, 2018), few studies in the literature are represented the utilization of VB₁ as a catalyst (Nezhad, 2013 and Pourjavadi, 2014). Although, its high water solubility nature and reusability poses as a biocatalyst endure it a desirable green catalyst. VB₁ as a biodegradable and green catalyst was stimulated some organic reactions like synthesis of pyrimidinones, acetoin formation, dihydropyridine, quinoxaline preparation and pyrimido benzothiazole derivatives (Rahman, 2018, Helby, 2019, Narayanan, 2012 and Nongrum, 2016).

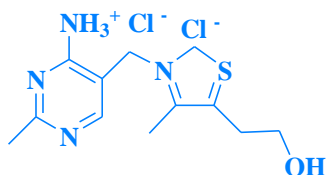


Figure 1. Structure of Vitamin B₁

Unlike this, agglomeration and surface oxidation of chemically very active unprotected magnetic nanoparticles (MNPs) result in a significant loss in magnetic catalytic activity, surface area, dispersibility, and properties. To overcome this problem silica supported coating layer not only functionalize the nanoparticle along with stabilizes nano particles superficial with functional groups like thiol, carboxyl, amine and biological species. In view of high surface affinity of the MNPs on silica as a chemically biocompatible inert compound with strong surface area and excellent stability, so it is generally supported as a coating layer over the surface (Patil, 2016). Silica possesses biocompatibility, less economic, widely abundant, less toxic, chemically and thermally stable. Silica of nanoparticles imparts make higher porosity and the surface area with more number of silanol (Si-OH) moieties reclining on surface area are able to be converted by different kinds of organic molecules for various purposes like coating, catalysis and separation etc (Esfandiary, 2020). Coating of silica recline on the superficial of biocompatible magnetic nanoparticles can effectively enhance the depuration of the nanocatalyst after finishing the reaction.

Benzothiazoles are a representative class of heterocyclic compound comprised fusion of benzene and thiazole ring system (Gjorgjieva, 2018). Benzothiazoles have exhaustive for transformed several biological activities corresponds antimicrobial (Singh, 2016, Haroun, 2018 and 2019), anticonvulsant (Shukla, 2016), antidiabetic (Abbasi, 2014), anti-tumor (Williams, 2020 and Pugh, 2020), antiviral (Azzam, 2020), antitubercular (Stokes, 2020), anti-inflammatory (Kumar, 2021), antiasthmatic (Costanzo, 2003), anthelmintic (Mohsen, 2017), antioxidant (Payaz, 2018), and so forth. There are several benzothiazole approved drugs such as ethoxzolamide (**A**, as diuretic), riluzole (**B**, as anticonvulsant), TCMTB (**C**, as fungicide), pramipexole (**D**, as antiparkinsonian), zopolrestat (**E**, as antidiabetic), viz., available in the market as shown in Figure 2. VB₁ was immobilized lying on the superficial of Fe₃O₄@SiO₂ core shell nanoparticles and induce further synthesis of benzothiazole derivatives. As it was mentioned above, the designed and synthesized benzothiazoles derivatives are more expected to have strong binding interactions with the active site of aminoacids of the influenza virus inhibition.

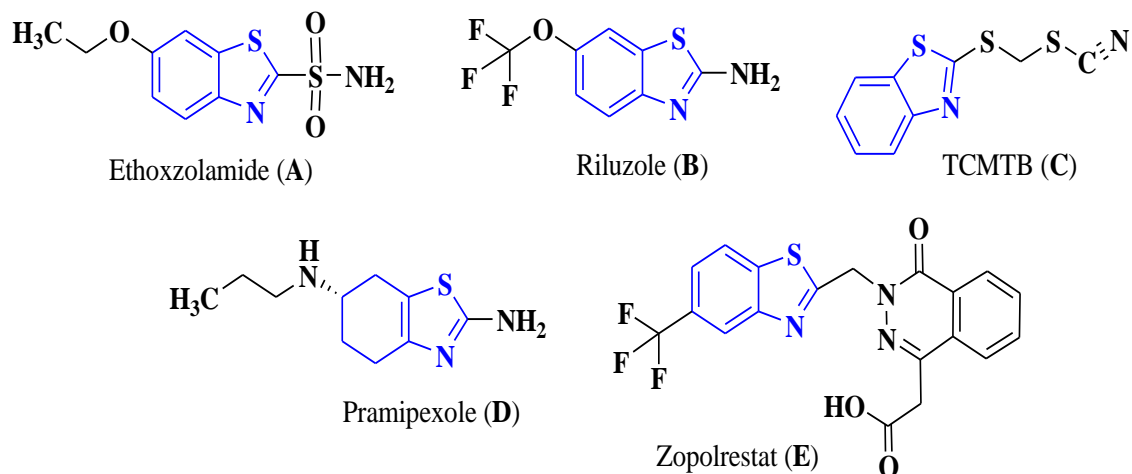


Figure 2. Marketed drugs containing the benzothiazole moiety

In extension of the work to promote novel catalysts for synthesis of benzothiazole derivatives, in view of this a moderate, potent, and eco friendly benign approach for the benzothiazole ring condensation in presence of nanosized particle catalyzed organic reactions, so considered the usage of VB₁ as an organocatalyst indulge on silica-sustained γ -Fe₂O₃ nanoparticle (γ -Fe₂O₃@SiO₂@Vitamin B₁). The conflicting of our present research work, we have designed benzothiazole scaffolds developed by molecular docking studies by employing Auto Dock tools 1.5.6 and molecular dynamics with Cresset Flare. The outcomes revealed that the recently structured benzothiazoles ancillaries showed significant activity with influenza virus protein. The docking results (i.e., interacting amino acids, binding score energy, distance and types of interactions) specifies the inhibitory effects of compounds in the protein using docking simulation.

2. Experimental

2.1 Materials and physical measurements:

All the chemicals and solvents were purchased with analytical grade and use directly without purification. FT-IR spectrum was recorded above the region 400–4000 cm⁻¹ on a Bruker, FT-IR apparatus using potassium bromide disks. Proton NMR (400 MHz) and ¹³C NMR (100 MHz) spectrum were obtained on a Bruker DRX400 spectrometer in DMSO and CDCl₃ solvents. The powder X-ray spectrum was depicted at room temperature on Bruker SMART APEX II CCD replenish with a graphite monochromator. The morphology nature of the nanoparticles was investigated with transmission electron microscopy using TEM (JEOL 2100). A minute quantity of diluted sample dissolved in alcohol was spotted on a TEM grid. Mass spectra were depicted on a Perkin Elmer, Calrus 680 GC-MS spectrometry.

2.2 Computational details and Ligand preparation

The computational assumes, were performed on an Intel (R) Core (TM) i3 processor with a memory of 8.0 GB RAM running on Windows 10 operating system. Molecular docking calculations were done by MGL tools 1.5.6, Auto Dock tools 1.5.6 and Auto Dock Vina packages (Molecular Graphics Laboratory (MGL), Scripps Research Institute, North Torrey Pines Road 10550, La Jolla, California, 92037) for predicting the accuracy of protein-ligand interaction. The ligand structures of these molecules were drawn with ChemDraw Ultra 4.0 software, then it was changed to reliable 3D conformations produced and the energies were moderated using DSV. The fetched files were saved in MDL Molfile (.mol) format and changed to .pdb file format respectively. Further, they were optimized and visualized with the aid of BIOVIA Discovery Studio Visualizer v16.1.0, (Dassault Systems Biovia software).

2.3 Protein structure preparation

The crystal arrangement of influenza virus protein PB2 complex (PDB ID: 5EG7, 1.40 Å) were retrieved from the source of Research Collaboratory for Structural Bioinformatics (RCSB) Protein Data Bank (<https://www.rcsb.org>) (Severin, 2016). The protein complex was extracted and prepared in protein training wizard, removed water molecules distantly around 5 Å of the binding site, further added polar hydrogen atoms and it was minimized. The 3D molecular structures of the designed compounds were further developed and optimized by using Cresset's structure-based drug design suite Flare V4 software with the assertion to acceptable values of bonding interactions, bond angles, bond length, unusual bonding interactions have appropriate to the atoms occupying the same bonding site in different parts of the compound. The tolerance energy minimization program used with the Open MM toolkit having high performance GPU platform using the 'steepest descent algorithm' with an energy tolerance to choose the cut-off value of 0.10 kcal/mol with AM1-BCC partial charges and the maximum iterations were equilibrated upto 10000 steps with the time step of 200 ps. A molecular dynamics calculation was used to attain the structures with the lowest energy through the simulated annealing in Flare V4 software. The open trajectories were set to be generated every 2 fs and save every 2 ps. The molecular structure was heated at high temperature (300 K) for a certain time 20 ns (20000 ps) for computing the final configuration. By this way, the different energies were found more durable than the original structural parameters.

2.4 Molecular docking or structure-based drug design

The key goal of protein-ligand docking is an ideal tool that can recognize the interaction between the target site and ligand and binding mode of ligands with target protein. The docking experiments of the designed compounds (**3a-p**) (Scheme 2) demonstrated immense linking to the protein into the active site of influenza virus protein PB2 complex were performed by employing molecular modelling software Autodock tools (ADT) v.1.5.6 (<https://ccsb.scripps.edu/mgltools/>) and AutoDockVina (Trott, 2010). Initially, protein was discriminated by deletion of water molecules and addition of polar hydrogen atoms or Kollman charges. The nonpolar hydrogen's were combined by using ADT, Gasteiger charges were consigned saved as .pdbqt file format. For docking evaluation, a grid box size of 60 x 60 x 60 Å was shaped within the range X (-27.173 Å), Y (13.580 Å) and Z (3.453 Å) axis including the spacing of grid point was selected with 0.375 Å were saved as grid parameter file (.gpf) and docking parameter file (.dpf) formats for determining pre calculated grid maps. After end of the docking experiments, the ligands were ranked by energy (Grigoryan, 2012).

2.5 Molecular dynamics simulation analysis

The ligands **3a-p** were docked into active site of influenza virus protein PB2 complex (PDB ID: 5EG7) by using Autodock tools (ADT) v.1.5.6. The best-docked ligand-protein interactions were chosen decided and based on their dock score. The docked output structures have saved in the .pdbqt file format for investigating and calculating the different types of interactions like positive hydrogen-bonding, lipophilic, electrostatic forces and π - π interactions etc. involved in docking. The ligand-protein interactions were all represented and visualized on the basis of docking results BIOVIA Discovery Studio Visualizer v16.1.0 software (Hardianto, 2018) and molecular dynamic simulations by utilizing Cresset's Flare software. The docking score capacity is for the most entity dependent on the docking parameters like lipophilic pocket which is significant of the action. The improvement of the binding affinity evaluated with different ligands by hydrogen bonding and electrostatic forces are other parameters. Molecular dynamic simulation is also a process in every stage of novel drug discovery for improvement of folding and protein stability, conformational changes and molecular recognition, computation of large scale 'movement' of the complex and lead optimization (Bauer, 2019). The most important feature between molecular docking and the molecular dynamics simulations is the variable, moment in time. In contrast, the molecular dynamics highlight the complex shape that mutate with time, further they have compared to molecular docking

experiments may produce reduces the calculation capacity, increased time and complexity. So, a molecular dynamics simulation is a fundamental validation that prior to draw any confirmations with the docking results (Vivo, 2016). Molecular dynamics simulations have improve the prospective of lead optimization, binding ability, binding pocket of compounds and to determine molecules targeting the protein-protein interface.

2.6 Synthesis of Vitamin B₁ supported on γ -Fe₂O₃@SiO₂ (Scheme 1)

2.6.1 Synthesis of Fe₃O₄ MNP'S:

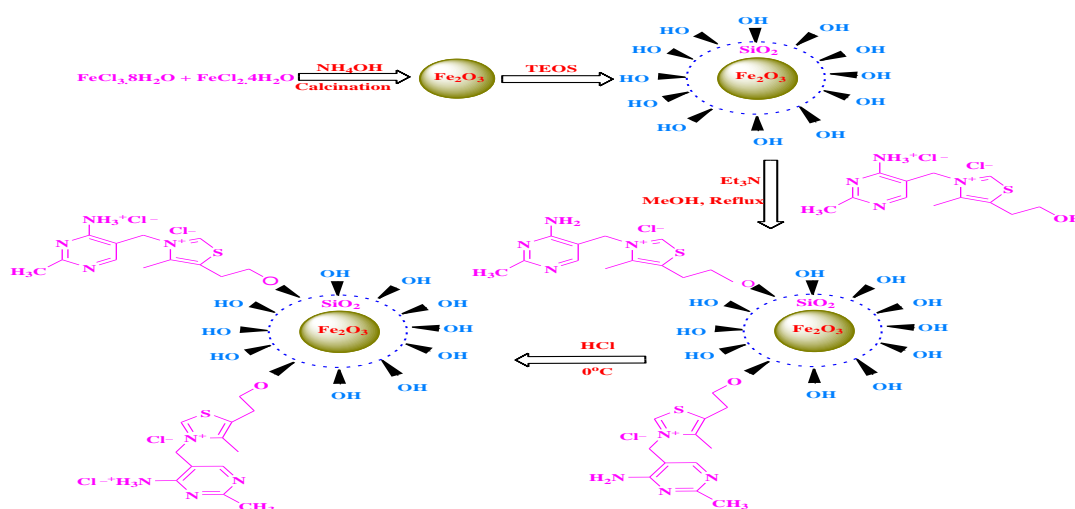
A Solution of FeCl₃.6H₂O (5 mmol) and FeCl₂.4H₂O (2.5 mmol) was dispersed in 100 ml deionized water under continuously stirred (800 rpm) and then added NH₄OH solution (25% w/w) was mixed to the resulting solution at room temperature until the pH was elevated to 11. Ammonium hydroxide solution was added to maintain the reaction pH in between 11 and 12 at this point a black precipitate was acquired. The resulting black suspension was treated vigorously stirred for 1 h and refluxed for 1 h. The suspension was purified and recrystallized from ethanol. Yield 98%, m.p. 94 °C.

2.6.2 The surface alteration of γ -phase Fe₂O₃ by tetraethyl orthosilicate (TEOS):

Coating of silica on the superficial of γ -phase ferrite nanoparticles was enacted by mixing ethanol (40 mL) to formed nanoparticles and then ignited for 1h at 40 °C temperature. Consequently, TEOS (10 mL) was charged to reaction content and then resulting solution was steadily stirred for 24 h. Coated silica nanoparticles were congregated by a external magnet and washed repeatedly four to five times with diethylether and ethanol and kept on drying in a vacuum at 100 °C for 12 h. Finally, the synthesized nano sized particles were ignited at 300 °C in a furnace for 3 h to modify Fe₂O₃@SiO₂ to formation of feasible γ -Fe₂O₃@SiO₂ nanoparticles. The suspension was purified and recrystallized from ethanol and yield found 95%.

2.6.3 Synthesis of γ -Fe₂O₃@SiO₂ coated with thiamine:

Synthesized γ -Fe₂O₃@SiO₂ (1 g) was suspended in methanol and Thiamine hydrochloride in the presence of triethylamine (1.2 mmol) for 8 h under reflux condition. Resultant MNP's were collected by magnetic decantation process and sequentially washed several times with ethanol, deionized water and methanol to eradicate triethylamine and any unretorted vitamin to get the free γ -Fe₂O₃@SiO₂@thiamine catalyst. The catalyst was purified and recrystallized from ethanol and yield found 90%.



Sc

heme 1. Synthesis of γ -Fe₂O₃@SiO₂ @ Vitamin B₁

2.6.4 Synthesis of γ -Fe₂O₃@SiO₂ @ Vitamin B₁:

To reinstate the acid activity formally neutralized by triethylamine and adds 2 mL hydrochloric acid (1 M) in diethylether and continuously stirred for 3 h. Synthesized MNP's were washed several times with deionized water and diethylether. Further, dried under Rotovac at 80 °C for 24 h and preferred catalyst was acquired. The catalyst was purified and recrystallized from ethanol and yield found 85%.

2.6.5 General procedure for preparation of Benzothiazole derivatives:

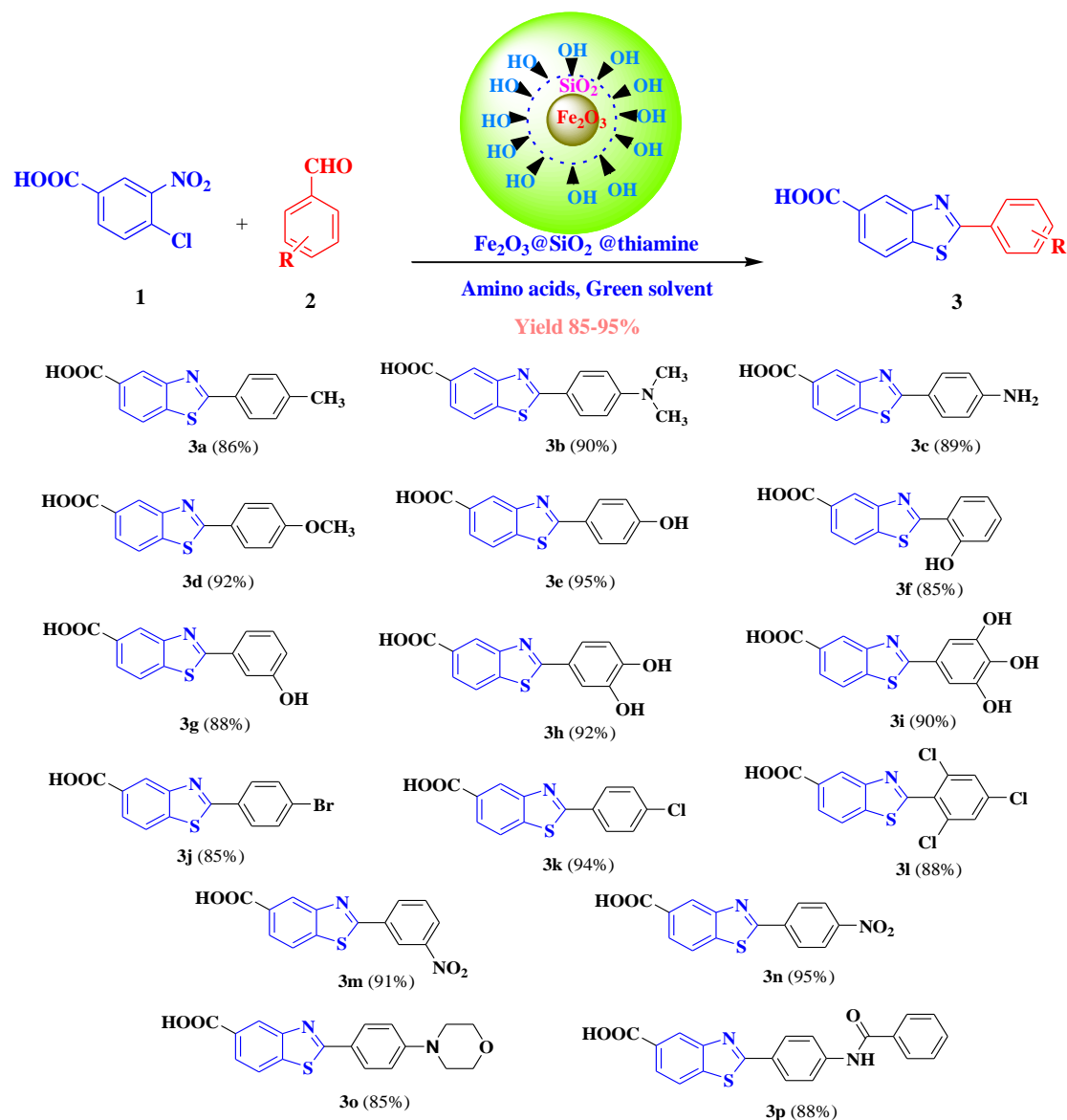
4-Chloro-3-amino-4-hydroxy benzoic acid (**1**) reacts with various substituted aliphatic/aromatic aldehydes (**2**), in presence of green solvent and heterogenous nanoorgano catalyst under various conditions. Purification of synthesized compounds was determined by melting point, thin layer and column chromatography. The synthetic method is shown in Scheme 2, to a mixture of 4-Chloro -3-amino-4-hydroxy benzoic acid (1.5 mmol), aromatic aldehydes (1.5 mmol), were dissolved in 25 ml of methanol, γ -Fe₂O₃@SiO₂ @ Vitamin B₁ (0.005 g) NPs was added and refluxed at 90 °C for a suitable time upto the reaction mixture become solidified. The development of the reaction was checked by TLC (n-hexane: ethyl acetate 7:3) and then the catalyst was effectively recovered by using an magnet and recycled for next synthesis. After elimination of catalyst, the content was make cool to room temperature and further, the crude products was washed by recrystallization from warm ethanol. The synthesized benzothiazole scaffolds (**3a-h**) were illustrated by FT-IR, Proton NMR, ¹³C NMR and Mass spectrum.

2-p-tolylbenzo[d]thiazole-5-carboxylic acid (**3a**):

Light yellow solid; Yield 86% (265.4 mg); m.p. 258-262 °C; FT-IR (KBr) ν_{\max} 3089 (C-H aromatic), 2987 (C-H aliphatic), 1675 (C=O) cm⁻¹. ¹H NMR (CDCl₃, 400 MHz) δ = 9.10 (s, 1H, CH, Benzothiazole), 8.42-8.33 (d, *J* = 8.25 Hz, 2H, H-6, H-7), 7.34-7.36 (d, *J* = 8.35 Hz, 2H, H-2, H-6), 7.12-7.14 (d, *J* = 8.15 Hz, 2H, H-3, H-5), 2.35 (s, 3H, -CH₃) ppm. ¹³C NMR (CDCl₃, 400 MHz) δ = 169.5 (C=O), 166.6 (C-2, Benzothiazole), 154.3 (C-4, Benzothiazole), 141.0 (C-9, Benzothiazole), 138.4 (CH, Ph), 129.6 (CH, Ph), 127.4 (CH, Ph), 126.1 (C-6, Ph), 122.6 (C-7, Ph), 121.8 (C-8, Ph), 24.3 (CH₃) ppm. HRMS (ESI): (*m/z*) calculated for C₁₅H₁₁NO₂S [M+H]⁺ : 270.0544; Found, 269.0510. Analytical cal. C₁₅H₁₁NO₂S: C, 66.89; H, 4.12; N, 5.20. Found: C, 66.32; H, 4.19; N, 5.09.

2-(4-(dimethylamino) phenyl) benzo[d]thiazole-5-carboxylic acid (**3b**):

Light cream colour solid; Yield 90% (315.6 mg); m.p. 264-268 °C; FT-IR (KBr) ν_{\max} 3358 (NH), 3085 (C-H aromatic), 2984 (C-H aliphatic), 1698 (C=O) cm⁻¹. ¹H NMR (CDCl₃, 400 MHz) δ = 9.12 (s, 1H, CH, Benzothiazole), 8.44-8.33 (d, *J* = 8.15 Hz, 2H, H-6, H-7), 7.30-7.34 (d, *J* = 8.15 Hz, 2H, H-2, H-6), 6.62-6.66 (d, *J* = 7.85 Hz, 2H, H-3, H-5), 2.85 (s, 6H, N(-CH₃)₂) ppm. ¹³C NMR (CDCl₃, 400 MHz) δ = 169.4 (C=O), 166.8 (C-2, Benzothiazole), 154.2 (C-4, Benzothiazole), 149.6 (C-6, Ph), 141.4 (C-9, Benzothiazole), 128.4 (CH, Ph), 127.6 (CH, Ph), 122.4 (CH, Ph), 122.6 (C-7, Ph), 121.8 (C-8, Ph), 40.3 (CH₃) ppm. HRMS (ESI): (*m/z*) calculated for C₁₆H₁₄N₂O₂S [M+H]⁺ : 298.0776; Found, 299.3596. Analytical cal. C₁₆H₁₄N₂O₂S: C, 64.41; H, 4.73; N, 9.39. Found: C, 64.32; H, 4.58; N, 9.49



2-(4-aminophenyl) benzo[d]thiazole-5-carboxylic acid (3c):

White solid; Yield 89% (286.8 mg); m.p. 214-218 °C; FT-IR (KBr) ν_{\max} 3348 (NH), 3096 (C-H aromatic), 2965 (C-H aliphatic), 1674 (C=O) cm^{-1} . ^1H NMR (CDCl_3 , 400 MHz) δ = 9.14 (s, 1H, CH, Benzothiazole), 8.33-8.44 (d, J = 8.25 Hz, 2H, H-6, H-7), 7.20-7.26 (d, J = 8.25 Hz, 2H, H-2, H-6), 6.52-6.54 (d, J = 8.15 Hz, 2H, H-3, H-5), 4.05 (s, 2H, NH_2) ppm. ^{13}C NMR (CDCl_3 , 400 MHz) δ = 169.2 (C=O), 166.4 (C-2, Benzothiazole), 154.4 (C-4, Benzothiazole), 148.4 (C-6, Ph), 141.2 (C-9, Benzothiazole), 128.2 (CH, Ph), 127.4 (CH, Ph), 123.5 (CH, Ph), 122.6 (CH, Ph), 121.8 (C-8, Ph) ppm. HRMS (ESI): (m/z) calculated for $\text{C}_{14}\text{H}_{10}\text{N}_2\text{O}_2\text{S}$ [$\text{M}+\text{H}$] $^+$: 270.0464; Found, 270.6064. Analytical cal. $\text{C}_{14}\text{H}_{10}\text{N}_2\text{O}_2\text{S}$: C, 62.21; H, 3.73; N, 10.36. Found: C, 62.28; H, 3.58; N, 10.45.

2-(4-methoxyphenyl) benzo[d]thiazole-5-carboxylic acid (3d):

Cream colour solid; Yield 92% (265.8 mg); m.p. 245-256 °C; FT-IR (KBr) ν_{\max} 3098 (C-H aromatic), 2954 (C-H aliphatic), 1684 (C=O) cm^{-1} . ^1H NMR (CDCl_3 , 400 MHz) δ = 9.12 (s, 1H, CH,

Benzothiazole), 8.36-8.42 (d, $J = 8.20$ Hz, 2H, H-6, H-7), 7.32-7.38 (d, $J = 8.15$ Hz, 2H, H-2, H-6), 6.82-6.86 (d, $J = 8.15$ Hz, 2H, H-3, H-5), 3.76 (s, 3H, -OCH₃) ppm. ¹³C NMR (CDCl₃, 400 MHz) $\delta = 169.4$ (C=O), 166.2 (C-2, Benzothiazole), 160.7 (CH₃), 154.2 (C-4, Benzothiazole), 141.0 (C-9, Benzothiazole), 128.5 (CH, Ph), 127.4 (CH, Ph), 122.6 (CH, Ph), 121.8 (C-8, Ph), 54.8 (CH₃) ppm. HRMS (ESI): (m/z) calculated for C₁₅H₁₁NO₃S [M+H]⁺ : 285.0468; Found, 285.2804. Analytical cal. C₁₅H₁₁NO₃S: C, 64.25; H, 3.86; N, 10.46. Found: C, 64.28; H, 3.68; N, 10.40.

2-(4-hydroxyphenyl) benzo[d] thiazole-5-carboxylic acid (3e):

Light cream colour solid; Yield 95% (288.6 mg); m.p. 268-276 °C; FT-IR (KBr) ν_{\max} 3065 (C-H aromatic), 2986 (C-H aliphatic), 1645 (C=O) cm⁻¹. ¹H NMR (CDCl₃, 400 MHz) $\delta = 9.10$ (s, 1H, CH, Benzothiazole), 8.33-8.42 (d, $J = 8.10$ Hz, 2H, H-6, H-7), 7.30-7.34 (d, $J = 8.25$ Hz, 2H, H-2, H-6), 6.76-6.84 (d, $J = 8.45$ Hz, 2H, H-3, H-5), 5.06 (s, 1H, -OH) ppm. ¹³C NMR (CDCl₃, 400 MHz) $\delta = 169.4$ (C=O), 166.6 (C-2, Benzothiazole), 158.7 (C-4, Ph), 154.3 (C-4, Benzothiazole), 141.0 (C-9, Benzothiazole), 128.9 (CH, Ph), 127.4 (C-7, Ph), 121.8 (C-8, Ph), 116.4 (CH, Ph) ppm. HRMS (ESI): (m/z) calculated for C₁₄H₉NO₃S [M+H]⁺ : 271.0803; Found, 273.0112. Analytical cal. C₁₄H₉NO₃S: C, 61.98; H, 3.34; N, 5.16. Found: C, 62.28; H, 3.85; N, 5.36.

2-(2-hydroxyphenyl) benzo[d] thiazole-5-carboxylic acid (3f):

Light yellow colour solid; Yield 85% (252.8 mg); m.p. 270-274 °C; FT-IR (KBr) ν_{\max} 3064 (C-H aromatic), 2980 (C-H aliphatic), 1642 (C=O) cm⁻¹. ¹H NMR (CDCl₃, 400 MHz) $\delta = 9.12$ (s, 1H, CH, Benzothiazole), 8.34-8.38 (d, $J = 8.15$ Hz, 2H, H-6, H-7), 7.32-7.34 (d, $J = 8.15$ Hz, 2H, H-2, H-6), 6.74-6.80 (d, $J = 8.15$ Hz, 2H, H-3, H-5), 5.08 (s, 1H, -OH) ppm. ¹³C NMR (CDCl₃, 400 MHz) $\delta = 169.4$ (C=O), 166.6 (C-2, Benzothiazole), 158.7 (C-4, Ph), 154.3 (C-4, Benzothiazole), 141.0 (C-9, Benzothiazole), 128.9 (CH, Ph), 127.4 (C-7, Ph), 121.8 (C-8, Ph), 116.4 (CH, Ph) ppm. HRMS (ESI): (m/z) calculated for C₁₄H₉NO₃S [M+H]⁺ : 271.0803; Found, 272.0112. Analytical cal. C₁₄H₉NO₃S: C, 61.98; H, 3.34; N, 5.16. Found: C, 62.28; H, 3.85; N, 5.36.

2-(3-hydroxyphenyl) benzo[d] thiazole-5-carboxylic acid (3g):

Cream colour solid; Yield 88% (252.8 mg); m.p. 272-276 °C; FT-IR (KBr) ν_{\max} 3072 (C-H aromatic), 2864 (C-H aliphatic), 1654 (C=O) cm⁻¹. ¹H NMR (CDCl₃, 400 MHz) $\delta = 9.14$ (s, 1H, CH, Benzothiazole), 8.36-8.34 (d, $J = 8.25$ Hz, 2H, H-6, H-7), 7.34-7.38 (d, $J = 8.25$ Hz, 2H, H-2, H-6), 6.84-6.88 (d, $J = 8.15$ Hz, 2H, H-3, H-5), 5.06 (s, 1H, -OH) ppm. ¹³C NMR (CDCl₃, 400 MHz) $\delta = 169.6$ (C=O), 166.4 (C-2, Benzothiazole), 157.8 (C-4, Ph), 156.3 (C-4, Benzothiazole), 142.6 (C-9, Benzothiazole), 126.4 (CH, Ph), 125.2 (C-7, Ph), 121.4 (C-8, Ph), 115.6 (CH, Ph) ppm. HRMS (ESI): (m/z) calculated for C₁₄H₉NO₃S [M+H]⁺ : 271.0803; Found, 272.0112. Analytical cal. C₁₄H₉NO₃S: C, 61.98; H, 3.34; N, 5.16. Found: C, 62.28; H, 3.85; N, 5.36.

2-(3,4-dihydroxyphenyl) benzo[d] thiazole-5-carboxylic acid (3h):

Light cream colour solid; Yield 92% (282.6 mg); m.p. 265-270 °C; FT-IR (KBr) ν_{\max} 3068 (C-H aromatic), 2874 (C-H aliphatic), 1658 (C=O) cm⁻¹. ¹H NMR (CDCl₃, 400 MHz) $\delta = 9.14$ (s, 1H, CH, Benzothiazole), 8.34-8.36 (d, $J = 8.25$ Hz, 2H, H-6, H-7), 7.30-7.36 (d, $J = 8.25$ Hz, 2H, H-2, H-6), 6.82-6.86 (d, $J = 8.15$ Hz, 2H, H-3, H-5), 5.06 (s, 2H, -OH) ppm. ¹³C NMR (CDCl₃, 400 MHz) $\delta = 169.4$ (C=O), 165.4 (C-2, Benzothiazole), 158.2 (C-4, Ph), 157.6 (C-4, Benzothiazole), 143.4 (C-9, Benzothiazole), 126.4 (CH, Ph), 125.2 (C-7, Ph), 122.1 (C-8, Ph), 116.8 (CH, Ph) ppm. HRMS (ESI): (m/z) calculated for C₁₄H₉NO₄S [M+H]⁺ : 287.0608; Found, 286.9112. Analytical cal. C₁₄H₉NO₄S: C, 61.98; H, 3.34; N, 5.16. Found: C, 62.28; H, 3.85; N, 5.36.

2.6.6 Catalyst loading and choice of solvent

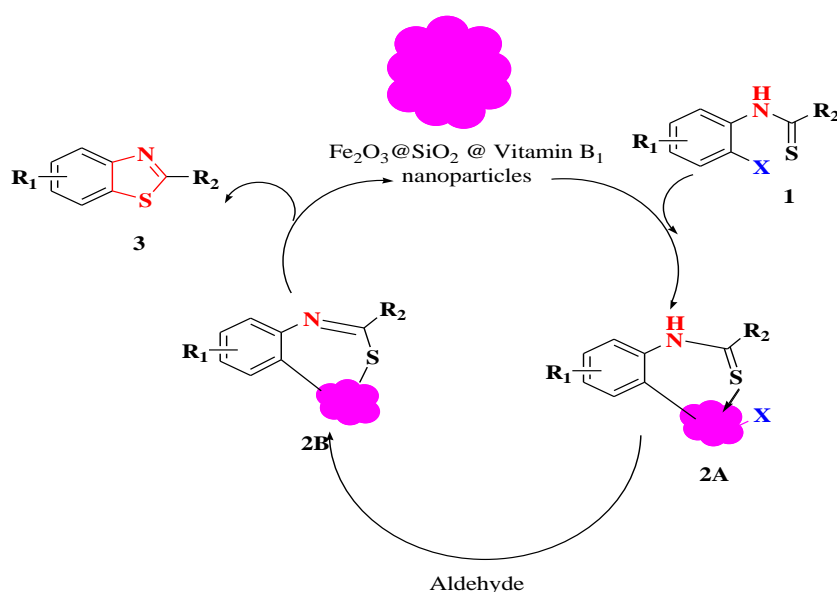
It is noticeable that effect of catalyst loading to approximate amounts of $\gamma\text{-Fe}_2\text{O}_3@\text{SiO}_2 @ \text{Vitamin B}_1$ on the consequence of the ideal reaction was also examined. Elevated loading of the nanocatalyst from 1 to 12 mol% for a constant reaction time revealed that 6 mol% of $\gamma\text{-Fe}_2\text{O}_3@\text{SiO}_2 @ \text{Vitamin B}_1$ in methanol was the ideal catalyst ratio intended for alteration leads to significant yield of the product. Smaller catalyst loadings give fewer yields, however larger loadings did not induce a prominent raise in yield of the product. The reaction was then carrying out in common solvents in presence of 6 mol% $\gamma\text{-Fe}_2\text{O}_3@\text{SiO}_2 @ \text{Vitamin B}_1$. The synthesis did not succeed in the dichloromethane and water although the reaction progress well in ethanol and methanol. Consequently, methanol as the solvent of choice due to it's easily removal during the reaction.

2.6.7 Application of the catalyst

To a reaction mixture of 4-Chloro-3-amino-4-hydroxy benzoic acid (1.5 mmol), aromatic aldehydes (1.5 mmol), was added the $\gamma\text{-Fe}_2\text{O}_3@\text{SiO}_2 @ \text{vitamin B}_1$ (0.005 g) and agitated was maintained at room temperature for suitable time (TLC). After finishing of the reaction, add methanol to the reaction mixture to get rid of the catalyst by using the magnet. After wards add water (10 mL) and then phases were alienated. The organic phase was rinsed with Sodium hydrogen carbonate solution, brine, dried (Disodium sulfate decahydrate) and concentrated to provide the pure product. The purified products were illustrated by evaluation of their physical data with that of known compounds.

2.6.8 A tentative mechanistic pathway

According to the literature study and outcomes possible tentative mechanism for the synthesis of Benzothiazole derivatives has been shown in Scheme 3. Initially, $\text{Fe}_2\text{O}_3@\text{SiO}_2 @ \text{Vitamin B}_1$ nanocatalyst reacted with the starting compound to form intermediate compound 2A and then converted into 2B in the occurrence of aldehydes which carry out the catalytic activity by the reductive elimination of the condensed product.



Scheme 3. Plausible mechanism for the synthesis of benzothiazole derivatives

3. Results and Discussion

3.1 Molecular docking

The binding energies of ligands with active site of influenza virus protein PB2 complex (PDB ID: 5EG7) were studied and docking results have analyzed and mentioned in terms of docking score, H-bond energy, interaction energy and interacting amino acid residues present at the active site of protein. The least docking score which stated that enhanced approach of binding with protein were summarized in Table 1. In the current study, we found that docking studies exposed out of 16 designed compounds, only **3a**, and **3o** have shown higher score than the standard drug (Dock score: -7.5 kcal/mol and forms 1 hydrogen bonds with LYS376, amino acid residues). Similarly, **3g** and **3k** were found to bind active site of protein with ASN425 and GLU369 amino acid residues with binding energy Dock score: -7.4 kcal/mol (H-bond length 2.7 \AA). The best docked poses of the designed ligands **3a**, **3g**, **3k** and **3o** with dock score were shown in Fig. 3, 4, and 5. The docking outcomes exposes that the binding affinity is mainly attributable to lipophilic factors because of the presence of strong electron donating groups like ($-\text{CH}_3$, $-\text{Cl}$, $-\text{OH}$, morpholine) and heterocyclic rings. The major part of benzothiazoles is mainly found in the hydrophobic pocket.

The docking of ligand **3a** with the influenza virus protein PB2 complex with an inhibitor exposed that ligand **3a** show higher affinity interaction with affinity of -7.5 kcal/mol to the chain A of protein (Figure 3). Interactions with amino acids comprised LYS 376, in the form of significant hydrogen bonding between the ligand **3a** (in acid group of benzothiazole) and amino acid residue of protein. Some of the van der Waals interaction of ligand (carbonyl group) with HYS357 and PHE404 has been observed. The aromatic benzene ring shows pi-alkyl interaction with MET427, HYS357 and PHE404 respectively has been observed.

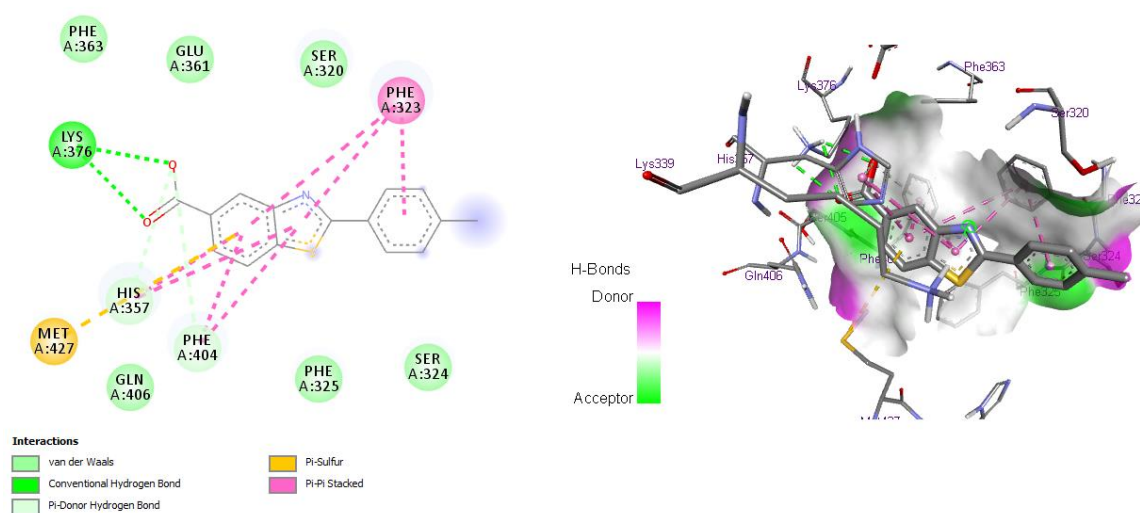


Figure 3. Docking study for ligand 3a with influenza virus protein PB2 complex (5EG7)

With two hydrogen bonding interactions, ligand **3o** showed promising activity with the influenza virus protein PB2 complex with the affinity of -7.5 kcal/mol. It confirmed that strong interaction with protein in the active site of binding pocket near to chain A of protein (Figure 4). The one hydrogen bonding interactions are mainly characterized between the hydroxyl group ($-\text{COOH}$) of benzothiazoles ring with LYS376. Further, a few number of pi-pi stacked interaction between the benzene ring and benzothiazoles ring with residues of PHE323, HIS357 and PHE404 respectively. Thus, it was observed that ligand **3o** favour influenza virus protein PB2 complex with an inhibitor.

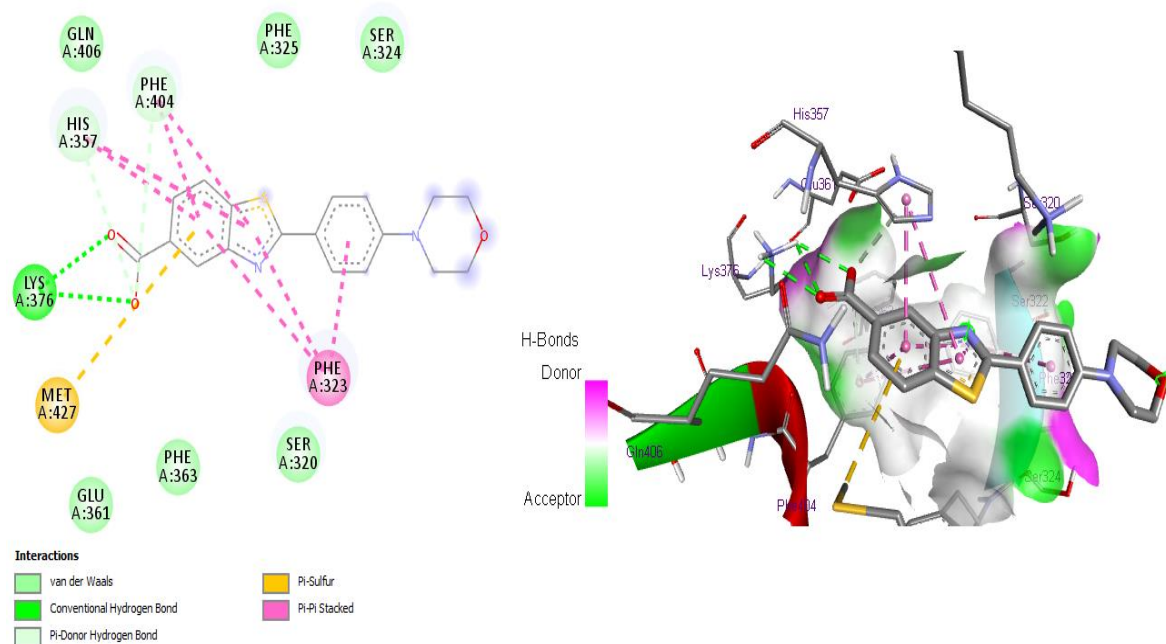


Figure 4. Docking study for ligand 3o with influenza virus protein PB2 complex (5EG7).

Table 1. The antiviral activity using Plaque reduction assay and docking studies for ligands 3a-p with influenza virus protein PB2 complex (5EG7).

Ligand	Minimum virus inhibitory concentration (µg/mL)	% of inhibition	Interacted amino acid residues with H-bonding	Interacting atoms (amino acid.....ligand)	Number of H-bonds formed	Binding energy (kcal/mol)	Interaction distance (Å)	Distance from rmsdl.b.
3a	>20	68	LYS376	Lys376.....O	3	-7.5	2.74, 2.55, 2.75	0.000
3b	>20	24	LYS376	Lys376.....O	3	-7.2	2.74, 2.56	0.000
3c	>40	18	LYS376	Lys376.....O	3	-7.3	2.75, 2.56, 2.73	0.000
3d	>20	32	LYS376	Lys376.....O	3	-7.1	2.74, 2.56, 2.73	0.000
3e	>16	47	LYS376, PHE404, GLN406	Lys376.....O Phe404.....O Gln406.....O	4	-6.9	2.94, 2.78, 3.19, 3.29	4.281
3f	>40	0	LYS339, LYS376, PHE404	Lys339.....O Lys376.....O Phe404.....O	4	-7.0	2.66, 2.83, 2.25, 3.27	2.998
3g	>20	3	LYS376, ASN425,	Lys376.....O	3	-7.4	2.30, 2.38, 3.24	2.083

			GLU361	Asn425.....O				
				Glu361.....O				
3h	>16	8	LYS376, GLU361, PHE404, GLN406	Lys376.....O Glu361.....O Phe404.....O Gln406.....O	5	-7.2	2.79, 2.68, 3.38, 3.15, 3.26	2.917
3i	>20	25	LYS376, GLU361, PHE404, GLN406	Lys376.....O Glu361.....O Phe404.....O Gln406.....O	6	-7.3	2.95, 2.27, 2.87, 2.83, 3.05, 3.23	1.364
3j	>8	36	LYS376	Lys376.....O	3	-7.3	2.75, 2.56, 2.76	0.000
3k	>16	29	LYS376	Lys376.....O	3	-7.4	2.74, 2.56, 2.73	0.000
3l	>16	13	ARG355	Arg355.....O	3	-7.3	1.94, 2.85, 2.81	0.000
3m	>16	10	SER324, LYS376	Ser324.....O Lys376.....O	4	-7.3	2.19, 2.40, 3.00	1.569
3n	>20	15	LYS376, ASN425, PHE404	Lys376.....O Asn425.....O Phe404.....O	4	-6.8	2.23, 2.80, 2.86, 3.24	2.765
3o	>20	62	LYS376	Lys376.....O	3	-7.5	2.74, 2.73, 2.55	3.276
3p	>20	15	SER324, ARG355,	Ser324.....O Arg355.....O	5	-6.4	1.80, 2.11, 1.65, 2.86, 2.97	5.786
Acyclovir	2.4	100	LYS376	Lys376.....O	4	-4.1	2.6, 2.8, 3.2	2.071

Similarly, results obtained by docking study of ligand **3g** and **3k** with influenza virus protein PB2 complex attributed several confirmations about the binding interaction (Figure 5). The best docking posture with protein showed binding affinity of -7.4 kcal/mol with a hydrogen bonding interaction between oxygen of carboxyl group in benzothiazole scaffold with GLU361, LYS376 and ASN425. Some of the pi-alkyl interactions of aromatic ring and imidazole rings with residues of MET427, HIS428, and PHE323 respectively. Furthermore, van der Waals interactions of ligands with carboxyl groups with the amino acid HIS 357. Based on this study results, it can opens the choice of research and applications of ligands **3a**, **3g**, **3k** and **3o** favour to act simultaneously on the influenza virus protein PB2 complex for binding in particular, for the treatment of influenza virus.

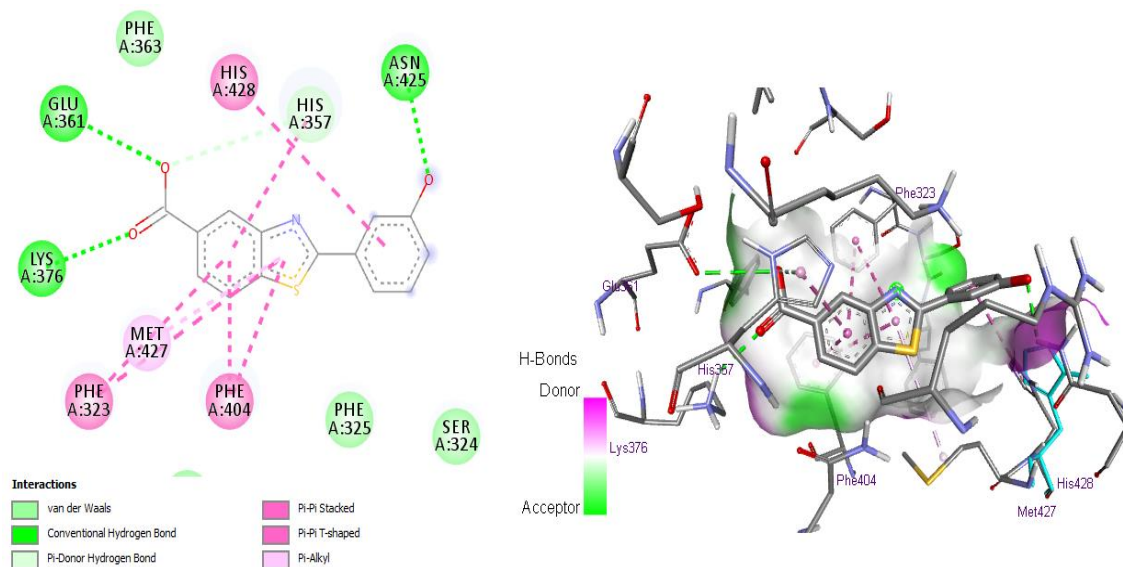


Figure 5. Docking study for ligand **3g** with influenza virus protein PB2 complex (5EG7).

3.2 Molecular dynamics simulation analysis

The ligands **3a-p** was docked into influenza virus protein PB2 complex. The least energy conformations of the ligands were best docked posture with target protein. Subsequently, the interaction between the ligand and amino acid residues were visualized in BIOVIA Discovery Studio Visualizer, the hydrogen bonding interactions were represented by dark green dash lines. Various amino acids engaged with protein ligand interactions have exposed as stick with different colour and binding pockets of proteins labelled by red colour sticks. The docking simulations of the binding interactions of relating compounds **3a-p** with the influenza virus protein PB2 complex are presented in the Table 1. In this study, best docking scores of protein-ligand complexes of four compounds **3a**, **3o**, **3g** and **3k** were selected and studied through molecular dynamics simulations. The endurance of RMSF computations for the protein-ligand complex (PDB ID: 5EG7) have progressively enlarged until the 1.56 Å then obtains stable till 10 ns, as represented as (Figure 6) formation of stable complex by the low RMSF through the simulation. Based on the best docking poses of selected ligands are remain stable from end to end, the MD simulations with slight adjusts and minimum fluctuations in the backbone RMSF within the satisfactory range.

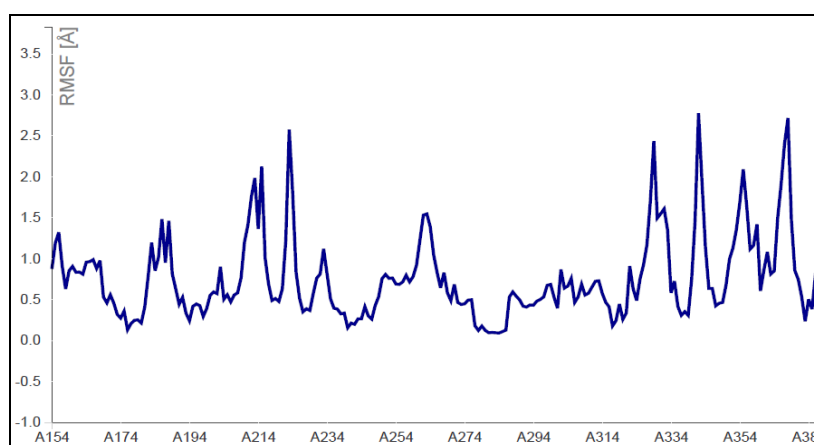


Figure 6. RMSF of protein and ligand backbones during the simulation.

The molecular dynamics simulations of influenza virus protein PB2 complex with ligand complexes of four compounds **3a**, **3o**, **3g** and **3k** were calculated on the basis of root-mean-square

deviation (RMSD) values have reflected the differentiation of compounds structures after comparing with the interactions of compounds with the protein and available structure in the crystal structure after docking. The docking results, are measured by RMSD values and considered reliable when the RMSD value is $< 1.56 \text{ \AA}$, and the binding interactions between protein-ligands complexes are calculated from 0 to 20000 ps, and is not significantly different. The RMSD values are steadily increased from 20 to 20000 ps and accomplished stable state throughout the simulation. During the molecular dynamics simulations the contacts of the simulation between 0 ns to 20 ns, various bonding interactions, such as hydrogen bonds, cation- π interactions, aromatic-aromatic interactions and the interaction between the active site of amino acids of protein and the atom of ligand as represented as (Figure 7).

The docking simulation of the interaction between compounds and the influenza virus protein PB2 complex; the inhibitory effects of compounds on the PDB 5EG7 protein, the order of active compounds inhibiting the protein is as follows: **3a** > **3o** > **3g** > **3k**.

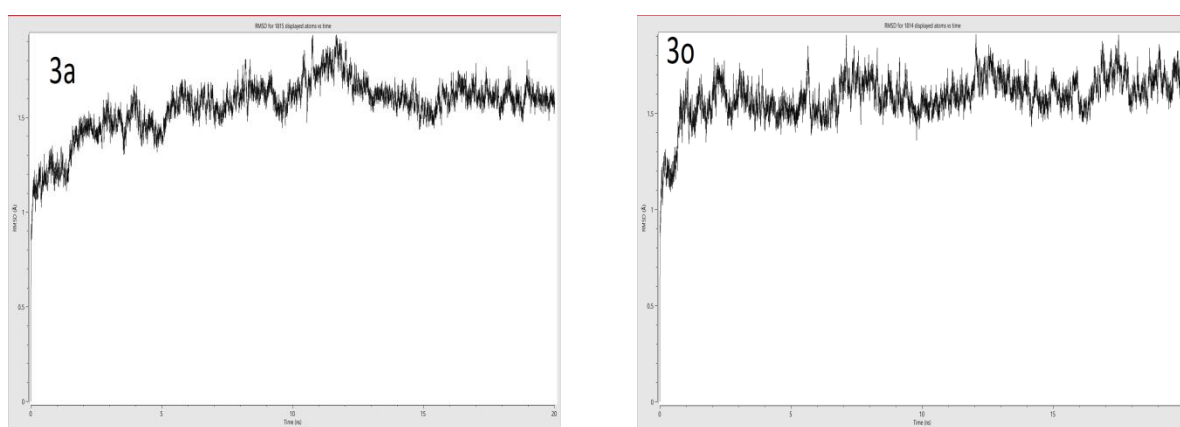


Figure 7. Plot of root mean square deviation (RMSD) during 20 ns in molecular dynamics simulation and binding interactions of influenza virus protein PB2 (5EG7) complex with ligands **3a** and **3o**.

3.3 Catalyst recycling

Additionally, recyclability of the $\gamma\text{-Fe}_2\text{O}_3@ \text{SiO}_2 @ \text{Vitamin B}_1$ nano catalyst was assess using 4-Chloro-3-amino-4-hydroxy benzoic acid reacts with various substituted aliphatic/aromatic aldehydes as a ideal reaction. After attaining the reaction, para super magnetic catalyst was isolated from the reaction, routinely, by using an external magnet field, then washed, dried and used for consequently further reaction run. The nanocatalyst was recycled upto the results were not good. In such a way, recyclability of our synthesized catalyst was explored (Figure 8). The catalyst affords excellent results for five succeeding cycles, after which there was deterioration in its catalytic efficiency.

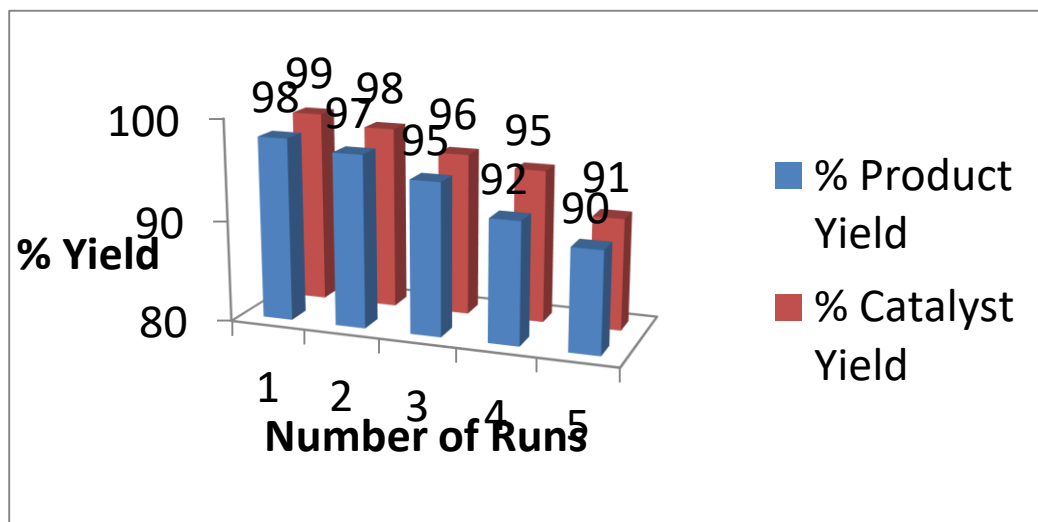


Figure 8. Recyclability of $\gamma\text{-Fe}_2\text{O}_3\text{@SiO}_2\text{@Vitamin B}_1$ nano catalyst

3.5 Transmission electron microscopy

Morphology of $\gamma\text{-Fe}_2\text{O}_3\text{@SiO}_2\text{@Vitamin B}_1$ was estimated using Transmission electron microscopy (TEM). The TEM image of the supported nanocatalyst confirmed that irregular sized particles owing to deposition of the silica on MNPs and illustrated that the existence of significant coated layers was shown in Figure 9. Various magnifications of TEM images showed that the nanoparticles are spherical in shape with small agglomeration and also Ferrite nanoparticles are spherical, closely dispersed, and well distributed with average size < 5 nm in diameter.

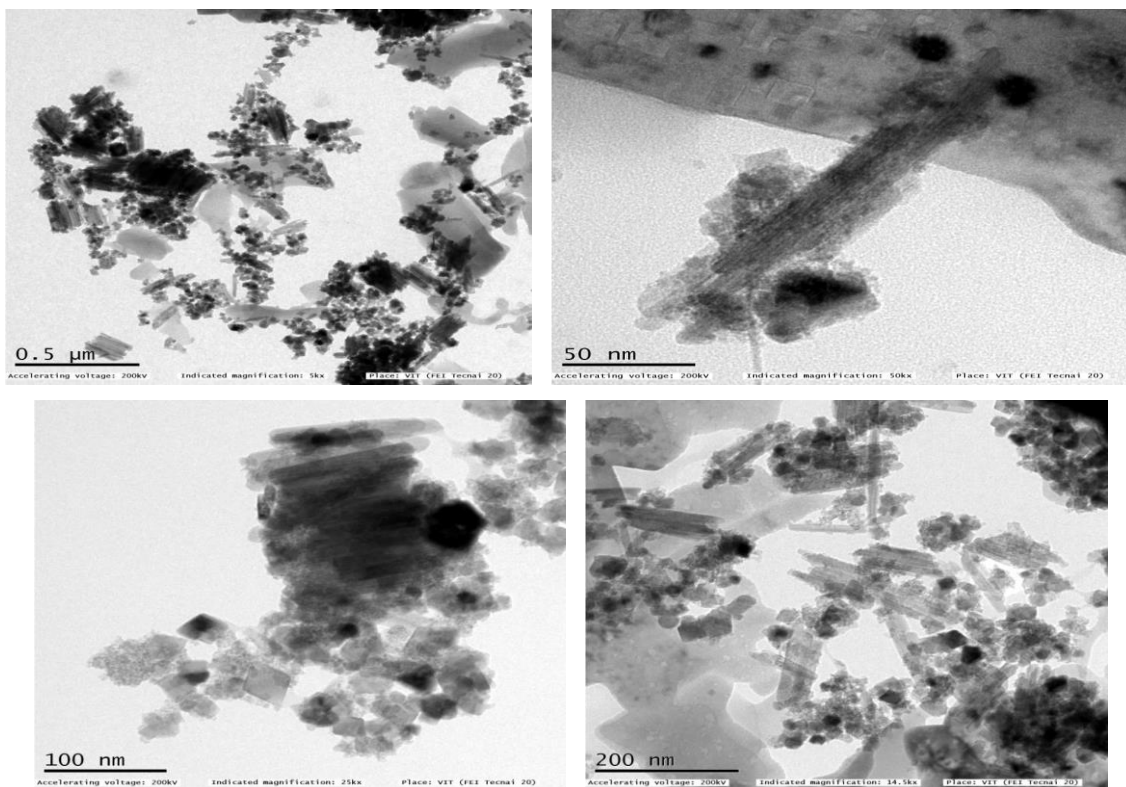


Figure 9. TEM analysis of the $\gamma\text{-Fe}_2\text{O}_3\text{@SiO}_2\text{@vitamin B}_1$.

3.6 X-ray diffraction (XRD)

Diffraction peaks observed in the region of 19.9°, 28.2°, 36.5°, 43.1°, 54°, 62.8°. The high-angle XRD pattern of the Fe₃O₄@SiO₂@Vitamin B₁ nanocatalyst is shown in Figure 10. This consequence indicates that the nanocomposite has been effectively synthesized without destruction of the crystal configuration of the Fe₃O₄ core.

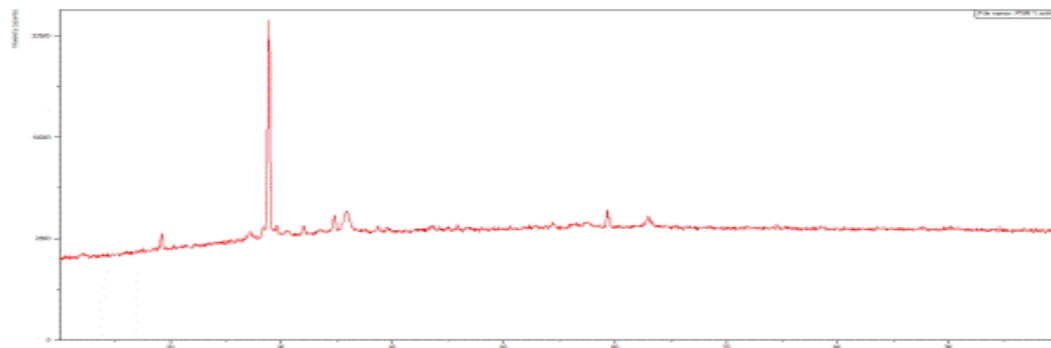


Figure 10. The X-ray diffraction patterns of the γ -Fe₂O₃@SiO₂@Vitamin B₁

3.7 Biological activity

Most of the synthesized benzothiazole compounds (**3a-p**) have been monitored for their inhibitory effect on influenza-3 virus in comparison with Acyclovir as a standard drug was concluded according to Plaque reduction assay (Hayden, 1980).

Minimum virus inhibitory concentrations and percentage of inhibition of these compounds were represented in the Table 1. Majority of the tested compounds showed weak to moderate activity. Among the compounds **3a** and **3o** were exhibited the most inhibitory effect on influenza-3 virus.

4. Conclusion

In summary, we have illustrated an effective one-pot two-component reaction involving different aldehydes and 4-Chloro-3-amino-4-hydroxy benzoic acid in a green approach with prominent yields for the synthesis of benzothiazole derivatives employing a high magnetically retrievable and high loaded organo nanocatalyst Fe₂O₃@SiO₂@Vitamin B₁. In consideration of the simplicity of the detachment of catalyst from the reaction content using bar magnet, without necessitate of further filtration procedure. Reusability of the biocatalyst was monitored until five times without substantial loss of its catalytic action. Further, the molecular docking study revealed that substituted benzothiazoles have shown significant binding affinity with active sites of target protein. The molecular dynamics simulation suggests that the active binding site of the most active compounds with the PDB- 5EG7 protein complex. Thus, *in-silico* structure based drug design strategy established in the present investigation make possible for identifying the hit compounds and furthermore elucidating for *in-vivo* and *in-vitro* assessment. From the analysis of biological activity and docking data, it revealed that the compounds **3a**, **3o**, **3g** and **3k** have significant inhibiting influenza virus protein PB2 activity with curative possibilities and are possibly helpful ligands after further refinement.

Acknowledgement

The authors acknowledge the University Grants Commission for financial assistance under UGC Minor Research Project (F.No.MRP-6803/16/UGC-SERO/30.06.2017)and Department of Science and Technology, New Delhi under DST-FIST program (F.No.SR/FST/College-280/18.11.2015) for

providing spectral analysis to Sri Venkateswara College of Pharmacy (Autonomous), RVS Nagar, Chittoor, Andhra Pradesh .

REFERENCES

1. Abbasi S, Mirza S, Rasheed S, Hussain S, Khan J A J, Khan K M, Perveen S and Choudhary M I, 2014. Benzothiazole derivatives: Novel inhibitors of methylglyoxal mediated glycation of proteins *in vitro*. *Medicinal Chemistry*, 10: 824-835. <https://doi.org/10.2174/1573406410666140331230953>.
2. Aghapoor K, Mohsenzadeh F and Talebian S, 2011. Vitamin B₁ as a metal-ion-free natural catalyst for sustainable quinoxaline ring condensation under sonochemical conditions. *Monatsh Chemistry*, 142, 619–624. <https://doi.org/10.1007/s00706-011-0487-5>.
3. Azizi K and Heydari A, 2014. Vitamin B₁ supported on silica-encapsulated γ -Fe₂O₃ nanoparticles: design, characterization and application as a greener biocatalyst for highly efficient acylation. *RSC Advances*, 4, 8812-8816. <https://doi.org/10.1039/C3RA46437G>.
4. Azzam R A, Elboshi H A and Elgemeie G H, 2020. Novel synthesis and antiviral evaluation of new benzothiazole-bearing n-sulfonamide 2-pyridone derivatives as usp7 enzyme inhibitors. *ACS Omega*, 5, 30023-30036. <https://doi.org/10.1021/acsomega.0c04424>.
5. Bauer M R and Mackey M D, 2019. Electrostatic complementarity as a fast and effective tool to optimize binding and selectivity of protein–ligand complexes. *Journal of Medicinal Chemistry*, 62, 3036-3050, <https://doi.org/10.1021/acs.jmedchem.8b01925>.
6. Choghamarani A G and Azadi G, 2016. Fe₃O₄@SiO₂@L-arginine@Pd(0): a new magnetically retrievable heterogeneous nanocatalyst with high efficiency for C–C bond formation. *Applied Organometallic Chemistry*, 30, 247–252. <https://doi.org/10.1002/aoc.3424>.
7. Choghamarani A G and Norouzi M, 2016. Synthesis and characterization of ionic liquid immobilized on magnetic nanoparticles: A recyclable heterogeneous organocatalyst for the acetylation of alcohols. *Journal of Magnetism and Magnetic Materials*, 401, 832-840. <https://doi.org/10.1016/j.jmmm.2015.10.044>.
8. Costanzo M J, Yabut S C, Almond H R, Gordon P A, Corcoran T W, Garavilla L, Kauffman J A, Abraham W M, Recacha R, Chattopadhyay D and Maryanoff B E, 2003. Potent, small-molecule inhibitors of human mast cell tryptase. Antiasthmatic action of a dipeptide-based transition-state analogue containing a benzothiazole ketone. *Journal of Medicinal Chemistry*, 46, 3865-3876. <https://doi.org/10.1021/jm030050p>.
9. Darabi H R, Aghapoor K, Farahani A D and Mohsenzadeh F, 2012. Vitamin B₁ as a metal-free organocatalyst for greener Paal–Knorr pyrrole synthesis. *Environmental Chemistry Letters*, 10, 369-375. <https://doi.org/10.1007/s10311-012-0361-7>.
10. Esfandiary N, Pazoki F, Nakisa A, Azizi K, Radfar I, Heydari A 2020 Silver chloride supported on Vitamin B₁-Organometallic magnetic catalyst: Synthesis, density functional theory study and application in A3-coupling reactions *Applied Organometallic Chemistry*, 34, e5725. <https://doi.org/10.1002/aoc.5725>.
11. Gjorgjieva M, Tomašič T, Kikelj D, and Mašič L P, 2018. Benzothiazole-based compounds in antibacterial drug discovery. *Current Medicinal Chemistry*, 25, 5218-5236. <https://doi.org/10.2174/0929867324666171009103327>.
12. Grigoryan A V, Wang H, and Cardozo T J, 2012. Can the energy gap in the protein-ligand binding energy landscape be used as a descriptor in virtual ligand screening? *PLoS One*, 7, e46532. <https://doi.org/10.1371/journal.pone.0046532>.

13. Gurav R, Surve S K, Babar S, Choudhari P, Patil D, More V, Sankpal S and Hangirgekar S, 2020. Rust-derived Fe₂O₃ nanoparticles as a green catalyst for the one-pot synthesis of hydrazinyl thiazole derivatives. *Organic Biomolecular Chemistry*, 18, 4575-4582. <https://doi.org/10.1039/d0ob00109k>.
14. Hardianto A, Liu F, Ranganathan S 2018 Molecular Dynamics Pinpoint the Global Fluorine Effect in Balanoid Binding to PKCε and PKA. *Journal of Chemical Information and Modeling*, 58, 511-519. <https://doi.org/10.1021/acs.jcim.7b00504>.
15. Haroun M, 2019. Novel hybrids of pyrazolidinedione and benzothiazole as tzd analogues: Rationale design, synthesis and *in vivo* anti-diabetic evaluation. *Medicinal Chemistry*, 15, 624-633. <https://doi.org/10.2174/1573406415666190515093657>.
16. Haroun M, Tratratt C, Kositzi K, Tsolaki E, Petrou A, Aldhubiab B, Attimarad M, Harsha S, Geronikaki A, Venugopala K N, Elsewedy H S, Sokovic M, Glamoclija J, Ciric A, 2018. New benzothiazole-based thiazolidinones as potent antimicrobial agents: Design, synthesis and biological evaluation, *Current Topics in Medicinal Chemistry*, 18, 75-87. <https://doi.org/10.2174/1568026618666180206101814>.
17. Hayden F G, Cote K M, Douglas R G, 1980. Plaque inhibition assay for drug susceptibility testing of influenza viruses. *Antimicrobial Agents and Chemotherapy*, 17(5), 865-870. <https://doi.org/10.1128/AAC.17.5.865>.
18. Helby A G E, Sakr H, Eissa I H, Abulkhair H, Karmalawy A A A and Adl K E, 2019. Design, synthesis, molecular docking, and anticancer activity of benzoxazole derivatives as VEGFR-2 inhibitors. *Arch Pharm Chemistry in Life Sciences*, 352, 113. <https://doi.org/10.1002/ardp.201900113>.
19. Kumar G and Singh N P, 2021, Synthesis, anti-inflammatory and analgesic evaluation of thiazole/oxazole substituted benzothiazole derivatives. *Bioorganic Chemistry*, 107, 104608-104620. <https://doi.org/10.1016/j.bioorg.2020.104608>.
20. Mohsen A, Omar M E, Aboulwafa O M, Issa D A E, El-Shoukrofy M S M, Amr M E, El-Ashmawy I M, 2017. Design, facile synthesis and anthelmintic activity of new O-substituted-6-methoxybenzothiazole-2-carbamates, Part II, *Medicinal Chemistry Communications*, 8, 1440-1451. <https://doi.org/10.1039/c7md00140a>.
21. Narayanan R, 2012. Synthesis of green nanocatalysts and industrially important green reactions. *Green Chemistry Letters and Reviews*, 5, 707-725. <https://doi.org/10.1080/17518253.2012.700955>.
22. Nezhad A K, Sarikhani S, Panahi F, 2013. A new silica-supported organocatalyst based on L-proline: An efficient heterogeneous catalyst for one-pot synthesis of spiroindolones in water. *Journal of Molecular Catalysis A: Chemical*, 379, 1-8, <https://doi.org/10.1016/j.molcata.2013.07.009>.
23. Nongrum R, Nongthombam G S, Kharkongor M, Rani J W S, Rahman N, Kathing C, Myrboh B, Nongkhlaw R, 2016. A nano-organo catalyzed route towards the efficient synthesis of benzo[b]pyran derivatives under ultrasonic irradiation. *RSC Advances*, 6, 108384-108392. <https://doi.org/10.1039/C6RA24108E>.
24. Patil A B, Bhanage B M, 2016. Sonochemistry: A greener protocol for nanoparticles synthesis. In: Aliofkhaezrai M. Handbook of Nanoparticles. *Springer*, 143-166. https://doi.org/10.1007/978-3-319-15338-4_4
25. Payaz D Ü, Küçükbay F Z, Küçükbay H, Angeli A, Supuran C T, 2018. Synthesis carbonic anhydrase enzyme inhibition and antioxidant activity of novel benzothiazole derivatives incorporating glycine, methionine, alanine, and phenylalanine moieties. *Journal of Enzyme*

- Inhibition and Medicinal Chemistry*, 34, 343-349, <https://doi.org/10.1080/14756366.2018.1553040>.
26. Porfiri P L, Gorgojo P, Miquel M G, 2020. Green solvent selection guide for biobased organic acid recovery. *ACS Sustainable Chemistry & Engineering*, 8, 8958-8969. <https://doi.org/10.1021/acssuschemeng.0c01456>.
 27. Pourjavadi A, Hosseini S H, Amin S S, 2014. Novel high loaded magnetic nanocatalyst based on multi-layered coating of poly(1-vinylimidazole). *Chemical Engineering Journal*, 247, 85-92. <https://doi.org/10.1016/j.cej.2014.02.080>.
 28. Pugh K W, Zhang Z, Wang J, Xu X, Munthali V, Zuo A, Blagg B S J, 2020. From bacteria to cancer: a benzothiazole-based dna gyrase b inhibitor redesigned for hsp90 c-terminal inhibition. *ACS Medicinal Chemistry Letters*, 11, 1535-1538. <https://doi.org/10.1021/acsmchemlett.0c00100>.
 29. Rafiee F, Mehdizadeh N, 2018. Palladium n-heterocyclic carbene complex of vitamin B₁ supported on silica-coated Fe₃O₄ nanoparticles: A green and efficient catalyst for c-c coupling. *Catalysis Letters*, 148, 1345-1354. <https://doi.org/10.1007/s10562-018-2363-y>.
 30. Rahman N, Nongthombam G S, Rani J W S, Nongrum R, Kharmawlong G K, Nongkhlaw R, 2018. An environment-friendly magnetic organo-nanomaterial as a potent catalyst in synthesis of pyranopyrazole derivatives. *Current Organocatalysis*, 5, 150-161. <https://doi.org/10.2174/2213337205666180731095751>.
 31. Roger J, Požgan F, Doucet H, 2009. Ligand-free palladium-catalyzed direct arylation of thiazoles at low catalyst loadings. *Journal of Organic Chemistry*, 74, 1179-1186. <https://doi.org/10.1021/jo802360d>.
 32. Severin C, Moura T R D, Liu Y, Li K, Zheng X and Luo M, 2016. The cap-binding site of influenza virus protein PB2 as a drug target. *Acta Crystallographica Section D*, 72, 245-253. <https://doi.org/10.2210/pdb5EG7/pdb>.
 33. Shukla R, Singh A P, Sonar P K, Mishra M, Saraf S K, 2016. Schiff bases of benzothiazol-2-ylamine and thiazolo[5,4-b] pyridin-2-ylamine as anticonvulsants: synthesis, characterization and toxicity profiling. *Central Nervous System Agents in Medicinal Chemistry*, 16, 240-248. <https://doi.org/10.2174/1871524916666160428110728>.
 34. Singh M, Singh S K, Gangwar M, Sellamuthu S, Nath G, Singh S K, 2016. Design, synthesis and mode of action of some new 2-(4-aminophenyl) benzothiazole derivatives as potent antimicrobial agents, *Letters in Drug Design & Discovery*. 13, 429-437. <https://doi.org/10.2174/1570180812666150821003220>
 35. Stokes S S, Vemula R, Pucci M J, 2020. Advancement of gyrb inhibitors for treatment of infections caused by mycobacterium tuberculosis and non-tuberculous mycobacteria. *ACS Infectious Diseases*, 6:1323-31. <https://doi.org/10.1021/acsinfecdis.0c00025>.
 36. Trott O, Olson A J, 2010. AutoDock Vina: improving the speed and accuracy of docking with a new scoring function, efficient optimization and multithreading. *Journal of Computational Chemistry*, 31, 455-461. <https://doi.org/10.1002/jcc.21334>.
 37. Vivo M D, Masetti M, Bottegoni G, Cavalli A, 2016. Role of molecular dynamics and related methods in drug discovery. *Journal of Medicinal Chemistry*, 59, 4035-4061. <https://doi.org/10.1021/acs.jmedchem.5b01684>.
 38. Williams N S, Gonzales S, Naidoo J, Cancel G R, Voruganti S, Panayotis P M, Theodoropoulos C, Geboers S, Chen H, Ortiz F, Posner B, Nijhawan D, Ready J M, 2020. Tumor-activated benzothiazole inhibitors of stearyl-coa desaturase. *Journal of Medicinal Chemistry*, 63, 9773-9786. <https://doi.org/10.1021/acs.jmedchem.0c00899>.

39. Zhang K, Suh J M, Choi J W, Jang H W, Shokouhimehr M, Varma R S, 2019. Recent advances in the nanocatalyst-assisted NaBH_4 reduction of nitroaromatics in water. *ACS Omega*. 4, 483-495. <https://doi.org/10.1021/acsomega.8b03051>.